J. Earth Syst. Sci. (2017) 126:47
DOI 10.1007/s12040-017-0832-0

A comparison of outer electron radiation belt dropouts during solar wind stream interface and magnetic cloud driven storms

O Ogunjobi[1,2,*], V Sivakumar[2] and Z Mtumela[2]

[1] *Center for Space Research, School for Physical and Chemical Sciences, North–West University, Potchefstroom 2520, South Africa.*
[2] *School of Chemistry and Physics, University of KwaZulu-Natal, Durban 4000, South Africa.*
**Corresponding author. e-mail: olakunle.ukzn@gmail.com*

MS received 15 February 2016; revised 27 December 2016; accepted 6 February 2017; published online 6 June 2017

Energetic electrons are trapped in the Earth's radiation belts which occupy a toroidal region between 3 and 7 R_E above the Earth's surface. Rapid loss of electrons from the radiation belts is known as dropouts. The source and loss mechanisms regulating the radiation belts population are not yet understood entirely, particularly during geomagnetic storm times. Nevertheless, the dominant loss mechanism may require an event based study to be better observed. Utilizing multiple data sources from the year 1997–2007, this study identifies radiation belt electron dropouts which are ultimately triggered when solar wind stream interfaces (SI) arrived at Earth, or when magnetic clouds (MC) arrived. Using superposed epoch analysis (SEA) technique, a synthesis of multiple observations is performed to reveal loss mechanism which might, perhaps, be a major contributor to radiation belt losses under SI and MC driven storms. Results show an abrupt slower decaying precipitation of electron peak (about 3000 counts/sec) on SI arrival within $5.05 < L < 6.05$, which persist till 0.5 day before gradual recovery. This pattern is interpreted as an indication of depleted electrons from bounce lost cone via precipitating mechanism known as relativistic electron microburst. On the other hand, MC shows a pancake precipitating peak extending to lower L (Plasmapause); indicating a combination of electron cyclotron harmonic (ECH) and whistler mode waves as the contributing mechanisms.

Keywords. Stream interfaces; magnetic clouds; magnetosphere; Earth's radiation belts; L-shell.

1. Introduction

The Earth's radiation belts were discovered over five decades ago. The radiation belts consist of an inner and outer zone separated by a region of lower density known as the slot (Van-Allen 1959). Electrons embedded in the solar wind can get ensnared by the Earth's magnetic field in the radiation belts. However, trapping in the inner belt is relatively steady, but the outer belt, which consists mainly of electron populations can be quite dynamic, reacting to changes in the Earth's magnetic field. Additionally, the waxing and waning of the outer belt's electron intensity depends on the solar wind forcing. Trapped energetic electrons can, rapidly, drop out of the outer radiation belt, depending on the specific geomagnetic conditions. Electrons from the outer radiation belt are often referred as killer electrons due to the damage which they can inflict on both objects (satellites) and men (Astronauts) in space (Horne 2007). The influence of solar wind dynamics on radiation belt population has

also subjected some of the basic physics principles into test. This is because one or more of the three adiabatic invariants (gyration, bounce and drift motions), governing the trapped energetic particles is/are often violated. However, if the Earth's magnetic field only varies slowly, then these particles would remain trapped in the belts. The benefits of the discovery and study of these belts are not confined to only commercial and military interests but also to the scientific community. The scientific interests, in particular, include understanding of the major loss mechanism to enable calculation of belts relaxation time, quantification of the electron loss during stormy times and the model calculations of upper atmospheric effects of the precipitating electrons; the so-called space weather prediction. Different geomagnetic storm-drivers or geospace events can induce significant dynamical changes in the outer belt resulting in dropouts of energetic particles. McIlwain (1972) was the first to observe decreases or dropouts in the trapped flux and suggested adiabatic effect as the cause, or actual losses through either precipitation into the atmosphere or lost through the magnetopause (known as magnetopause shadowing). Subsequent measurements (Thomsen *et al.* 1994) have shown that conditions for adiabatic mechanism are not generally present. Using satellite observation of energetic particles and field measurements, Thomsen *et al.* (1994) proposed that a strong field aligned current system together with the storm-enhanced ring current caused the compression of the local plasma sheet. This proposition was not fully consistent with the work of Onsager *et al.* (2002), which investigated the dependence of radiation belt electron dropouts on local time, radial distance, and particle-energy. Onsager *et al.* (2002) noted that the initial dropouts were controlled by the adiabatic response called Dst effect and that non-adiabatic, which involve interactions with various magnetospheric waves will result in eventual loss. This is followed by Meredith *et al.* (2003), who reported an electromagnetic ion cyclotron (EMIC) wave as the likely mechanism for pitch-angle scattering of electrons, but prescribed that energy >2 MeV will be needed for EMIC to act. In partial support for Meredith *et al.* (2003), Borovsky and Denton (2009) found that Dst effect plays an insignificant role during some specific geospace events. While the work of Meredith *et al.* (2003) generated much interest initially, it was later noted that dropouts can be frequent for electron energy <2 MeV. Morley *et al.* (2010) observed electron precipitation of >30 keV outside plasmapause in response to outer electron dropout and suggest relativistic electron microburst as one of the likely mechanisms responsible for such rapid dropouts.

Despite extensive work describing the dropout signature (e.g., Millan *et al.* 2002; O'Brien *et al.* 2004; Thorne *et al.* 2005; Millan and Thorne 2007) in response to geomagnetic storms, there seems to be no consensus regarding the most dominant mechanism in operation. According to Borovsky and Denton (2009), dropouts or lack of dropouts should be studied in different geospace events, particularly, in corotating interaction region (CIR) and coronal mass ejection (CME)-driven storms. This is because the high-speed-stream-driven storms or CIR are less variable than CME-driven storms.

Furthermore, the internal correlations between various parameters are one of the problems in the study of solar wind–magnetosphere coupling and responsible for shielding mechanism causing dropouts. For instance, Ogunjobi *et al.* (2014b) noted that within each of several geospace event structures, the magnetic fields might be of different origins and the solar wind parameters that control the solar wind–magnetosphere coupling might also have different behaviours. Thus the whole area is somewhat complex and needs a more specific comparative event-based study to be better observed. In this study, we focussed on only the outer electron radiation belt responses to solar wind stream interfaces (SI) and magnetic clouds (MC) driven storms.

The SI occurrence can be explained based on the non-uniformity (low and high speeds) in solar wind streams. The low speed stream originates from the vicinity of streamer belts while high speed stream came from the coronal holes. The point at which the passing high speed stream overtakes the trailing low speed stream is known as SI (Burlaga 1974). Due to the influence of the interplanetary magnetic field (IMF), the two flows cannot mix, making it to form a velocity shear at the interface point. The interface point delineates the dense plasma from less dense plasma. Also, SI is an attendant of CIR and its arrival at Earth Bow Shock Nose (BSN) can be recognized by the deflection of the solar wind azimuthal velocity from westward to eastward (Burlaga 1974). The MC, on the other hand, is a transient ejection in the solar wind, which is relatively characterized by a smooth rotation of the IMF, particularly the component perpendicular to the ecliptic plane, Bz (Lepping *et al.* 1997). MC can

simply be described as the region between the preceding half of the southward IMF and the trailing half, which contains a strong southward IMF peak or *vice versa*. Contrary to SI which is a subset of CIR, MC is an attendant of CME.

In this study, we examined, comparatively, possible mechanism in operation during outer electron radiation belt dropouts triggered by SI and MC. This is achieved by studying the characteristics of solar wind conditions and geophysical properties, determination of temporal and energy dependency of the dropouts, and investigation of ionospheric responses. Further, the results of this study will be taken into account in the development of our ongoing modified half-wave rectifier model for magnetospheric disturbance.

2. Datasets and event cleaning

Dropouts, due to SI and MC driven storms, were inspected and measured by the synchronous orbit particle analyzer (SOPA) instruments on Los Alamos National Laboratory (LANL) satellite. The interest in LANL is mainly the geosynchronous position above the Earth's surface and the wide coverage of magnetic local time. Geosynchronous Earth orbit (GEO), is essentially at the altitude of $L = 6.6$ (L is dipole magnetic field, which will be explained subsequently), which is in the boundary region of stable trapping for electrons. Apart from the morphology of this region, understanding the dynamics of electron dropouts from outer radiation belts requires knowledge of electron energy and its temporal evolution which SOPA instruments provide. Furthermore, because of its position, LANL can observe decrease in the energetic electron fluxes which is associated with the substorm growth phase (Belian *et al.* 1992). It is well known that dropout is due to the stretching of the magnetic field lines during the growth phase of substorm which is magnetically connected to the satellite in the more distant tail. This phenomenon is known as dispersionless injection which indicates that satellite is within the region of injection as in the case of LANL satellite. Seven LANL/SOPA equipped satellites, which cover wide range of magnetic local time, have been in operation since 1989. Data are mostly received from three or four satellites simultaneously. The satellites with SOPA instruments are 1989-046, 1990-080, 1991-095, 1994-084, LANL 97A, LANL 01A, and LANL 02A. For every operational satellite, flux data were normalized to obtain the same yearly averaged logarithm. It is possible to obtain logarithmic average by summation of log-fluxes divided by the number of satellites per time. The SOPA flux measurements used for study were from four electron channels 225–315, 315–500, 0.75–1.1 and 1.1–1.5 Mev. A comprehensive description of LANL/SOPA can be found elsewhere (Belian *et al.* 1992).

A low Earth orbit (LEO) satellite, National Oceanic and Atmospheric Administration/Polar Orbiting Environmental Satellites (NOAA/POES), is also employed. The POES, a polar-orbiting, Sun-synchronous, low-altitude (850 km) with a period of about 100 min satellite, has on-board the medium energy proton and electron detector (MEPED) that monitors the intensities of charged particle radiation at higher energies. POES 15, 16, 17, and 18 orbit both morning and afternoon sector of the earth in such a way that they pass over the poles, thus, it observes a wider range of magnetic field lines crossing the equator (in L-values) and covering the entire magnetic local time (MLT). Under adiabatic changes to the geomagnetic field, L is a conserved quantity (Roeder 1970). In a dipole magnetic field, L is the distance from the centre of the Earth to the equatorial crossing point of a given field line. The POES >30 keV electrons are ordered based on McIlwain L values from L. The McIlwain, L shell used in this study is calculated using the international geomagnetic reference field (IGRF) model from http://ngdc.noaa.gov. In this study, we projected the particle down to about 100 km, which is closer to the footprint of the magnetic field line, and then sort the measurement in a McIlwain L shell of ± 0.05L, starting from $L = 3$ to 8 (i.e., $L = 2.95-8.05$). This precaution is necessary because during intense geomagnetic storm, a GEO satellite can appear to be in $L = 5$ and be measuring at $L = 4$ (Varotsou *et al.* 2008). So, particular attention is focused on the $L = 4-7$. Although POES precipitating electron data is known of proton contamination (Rodger *et al.* 2010), we have however minimized the effect of proton contamination using first order correction. The fidelity of this correction can be found in Lam *et al.* (2010).

In this study, >30 keV electrons from MEPED have been used as an input to Monte Carlo Energy Transport model (MCETM) (see, Ogunjobi *et al.* 2014a, for details).

Geophysical parameters were obtained from the OMNI database (http://omniweb.gsfc.nasa.gov). The OMNI database is a multi-source dataset, which comprises measurements of near-Earth solar

wind, plasma, magnetic field and other geomagnetic parameters with coverage from November 1963. In other words, OMNI database consists of geomagnetic storms that were identified from the measurement of the global variation in the Earth's magnetic field at the Earth's bow shock nose. The dataset is created at National Space Science Data Center (NSSDC) by interspersing, after cross-normalizing, field and plasma data from each of several spacecrafts that contribute into the measurements (King and Papitashvili 2005; Ogunjobi *et al.* 2014a). From different parameters available at OMNI, only those that are relevant to characterizing the SI and MC were extracted as presented in section 3.

Also, we investigated the ionosphere at the time of the dropouts using ground-based riometers (Relative Ionospheric Opacity Meters) from the Finnish Riometer chain (http://www.sgo.fi/Data/Riometer/riometer.php) in the northern hemisphere. Remote sensing of electromagnetic waves of cosmic origin is a technique used in studying the state and the structure of the ionosphere (Behera *et al.* 2014). Riometers respond to the integrated absorption of cosmic ray noise through the ionosphere at heights where the electron (up to 30 keV) motion is collision dominated (Morley *et al.* 2010; Ogunjobi *et al.* 2014b). With such sensitivity, riometers data can be examined for ionospheric absorption at the time of dropouts and, by proxy, where the precipitation is localized.

2.1 *Events and measurement techniques*

Electron dropouts were selected by visual inspection of hourly quick look plots of SOPA electron fluxes at all energies and at all local times, using the onset of events as described in subsection 2.2. Dropouts events were collected from 1996 to 2007 in order to have a clear understanding of the variability of occurrence in maximum and declining phase of the solar activity. Events were classified as dropouts only when it satisfies the following criteria:

- when fluxes drop to background levels across a wide energy range (Belian *et al.* 1992; Fennell *et al.* 1996),
- when it is not double, that is, no immediate dropouts before and after,
- when there is no proton contamination. This is achieved by checking NOAA space environment (http://www.swpc.noaa.gov/ftpmenu/index.html.) for any known solar proton events.
- when there is a clear signal of either SI or MC. This is achieved by examining solar wind conditions and geomagnetic data on the day of dropout. It should also be noted that MC referred to in this study are of southward type.

204 dropouts were initially identified from 1996 to 2007. These events are subsets of catalogue of events found in Ogunjobi (2011). The selection criteria above were then applied. Seventeen were discarded as duplicates or due to other factors while 25 were eliminated as proton contaminated events and another 17 were avoided as unclear signature of SI or MC leaving a total of 145 cleaned dropouts from which 80 were classified as SI-driven dropouts and the balance were classified as MC dropouts. The cleaned events and associated solar wind structures are listed in table 1.

2.2 *SEA technique*

One method of composition of time series data is called superposed epoch analysis (SEA) technique. This technique is used to reveal consistent responses, relative to some repeatable phenomenon, in noisy data (Chree 1908). It consists of sorting data into categories (key events) and comparing means for different categories. The technique is such that data are averaged in relation to the event, the consistent signal will remain and random influences will tend to average out without any assumption of linearity. The reference time, zero epoch, allows one to investigate the onset of interplanetary sources and the initial part of the event because of the recurring nature of SIs and MCs, as storm drivers, they are amenable to SEA. The choice of reference (zero) time for SEA is important and substantially influences the results (Borovsky and Denton 2009). In this study, time series of the variables under investigation (SI and MC) are extracted from a window (±3 days) around the epoch and all the data (N) at a given time relative to epoch form the sample of events at that lag. The mean data ($\bar{D}$) at each epoch time (t) lag are then taken as measure of central tendency: $\bar{D}(t) = \frac{1}{N}\sum_{i=1}^{N} D_i(t)$ such that the fluctuations, as seen in figure 1, not consistent about the epoch cancel. In figure 1, the key day (D_0) is denoted as 0 epoch day in which case we obtained the sequence of means corresponding to 3 days prior to the key day and 3 days after the key day for 80 selected SI events. Note that the traces for some of the SI and MC events are superimposed by the other events in figure 1 (top and bottom panels), respectively.

Table 1. *Selected dropouts and associated solar wind structure from 1996–2007 used for study.*

Sl. no.	Year	DOY	SWS	Time (UT)	Sl. no.	Year	DOY	SWS	Time (UT)	Sl. no.	Year	DOY	SWS	Time (UT)
1	1996	13	MC	16:00	50	1999	298	MC	23:07	99	2004	42	SI	18:00
2	1996	56	SI	05:00	51	1999	311	SI	23:00	100	2004	69	MC	03:10
3	1996	63	MC	11:10	52	1999	337	SI	04:30	101	2004	96	SI	14:30
4	1996	100	MC	12:00	53	2000	22	MC	03:10	102	2004	199	SI	08:30
5	1996	185	MC	17:30	54	2000	43	MC	17:01	103	2004	220	MC	22:10
6	1996	242	SI	12:30	55	2000	52	MC	09:08	104	2004	243	SI	19:00
7	1996	319	SI	13:00	56	2000	145	MC	10:01	105	2004	287	SI	15:10
8	1996	360	MC	02:00	57	2000	154	SI	08:00	106	2004	304	SI	12:30
9	1997	10	MC	05:40	58	2000	178	MC	08:03	107	2005	2	SI	04:00
10	1997	36	SI	06:30	59	2000	193	MC	06:08	108	2005	29	SI	13:30
11	1997	42	MC	13:20	60	2000	279	SI	11:30	109	2005	49	MC	23:01
12	1997	66	SI	22:30	61	2000	287	MC	18:04	110	2005	64	SI	06:30
13	1997	87	SI	06:00	62	2000	302	MC	23.03	111	2005	95	SI	05:30
14	1997	111	MC	14:50	63	2000	319	SI	18:00	112	2005	110	SI	03:30
15	1997	121	SI	01:30	64	2000	360	SI	23:00	113	2005	119	MC	11:00
16	1997	135	MC	09:00	65	2001	21	SI	07:00	114	2005	128	SI	23:30
17	1997	159	MC	02:00	66	2001	24	MC	23.01	115	2005	140	SI	07:00
18	1997	188	SI	02:00	67	2001	78	MC	23:03	116	2005	174	SI	10:30
19	1997	240	MC	12:23	68	2001	212	SI	12:30	117	2005	269	SI	06:00
20	1997	246	MC	14:20	69	2001	217	SI	08:30	118	2005	281	SI	03:00
21	1997	274	MC	16:00	70	2001	254	SI	13:00	119	2005	304	MC	02:09
22	1997	318	SI	11:00	71	2001	281	SI	17:00	120	2005	317	MC	23:30
23	1997	326	MC	15:00	72	2001	305	SI	15:00	121	2005	361	SI	15:30
24	1997	364	MC	11:02	73	2002	59	MC	09:10	122	2006	16	MC	11:15
25	1998	8	MC	14:00	74	2002	89	SI	08:00	123	2006	26	SI	15:00
26	1998	16	SI	03:00	75	2002	103	MC	07:10	124	2006	36	MC	19:01
27	1998	48	MC	18:20	76	2002	131	SI	11:00	125	2006	65	MC	22:10
28	1998	59	SI	07:30	77	2002	159	SI	04:30	126	2006	95	SI	15:30
29	1998	63	MC	14:03	78	2002	247	SI	15:30	127	2006	124	SI	22:30
30	1998	80	SI	01:00	79	2002	277	MC	11:23	128	2006	219	SI	07:30
31	1998	101	MC	15:30	80	2002	300	SI	15:00	129	2006	231	MC	01:00
32	1998	122	MC	12:00	81	2002	322	MC	07:04	130	2006	239	MC	13:20
33	1998	157	SI	19:30	82	2002	325	SI	20:00	131	2006	260	SI	20:30
34	1998	186	MC	09:05	83	2002	341	SI	03:30	132	2006	267	SI	04:00
35	1998	218	MC	02:07	84	2002	360	SI	07:00	133	2006	293	MC	05:01
36	1998	239	MC	13:00	85	2003	3	SI	22:00	134	2006	301	SI	20:30
37	1998	268	MC	10:01	86	2003	8	MC	11:23	135	2006	314	SI	17:00
38	1998	280	SI	20:30	87	2003	29	SI	09:00	136	2007	15	MC	07:00
39	1998	292	MC	05:01	88	2003	58	MC	09:00	137	2007	29	SI	10:00
40	1998	317	MC	13:01	89	2003	88	MC	23:00	138	2007	59	SI	00:30
41	1998	357	SI	00:30	90	2003	92	SI	04:10	139	2007	84	SI	23:30
42	1998	363	MC	08:10	91	2003	192	SI	15:00	140	2007	91	SI	04:00
43	1999	4	SI	15:00	92	2003	207	SI	08:30	141	2007	127	SI	15:30
44	1999	13	MC	22:03	93	2003	230	MC	11:06	142	2007	237	SI	23:00
45	1999	49	MC	14.03	94	2003	233	SI	10:30	143	2007	263	SI	00:30
46	1999	55	SI	17:30	95	2003	260	SI	20:30	144	2007	290	SI	08:30
47	1999	106	MC	10:08	96	2003	287	SI	18:00	145	2007	324	SI	07:00
48	1999	210	MC	21:01	97	2003	324	MC	10:08					
49	1999	262	MC	01:09	98	2004	22	SI	21:30					

DOY is day of the year and SWS is solar wind structure. Epoch times for the MC are based on the start time for smooth rotation of IMB Bz whlie the epoch times for SI are identified to the nearest 30 minutes near the Earth's bow shock nose.

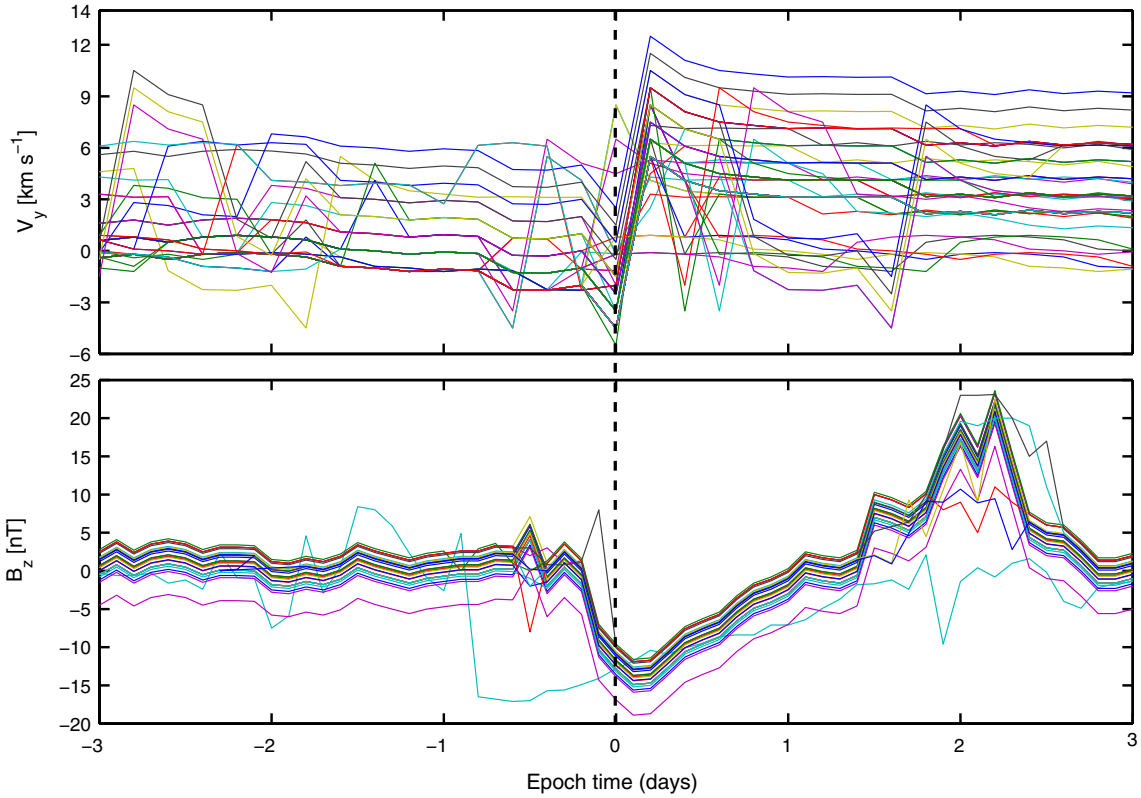

Figure 1. The solar wind azimuthal velocity (GSE-V_Y) for set of the 80 SI (top panel) and IMF Bz for the set of MC (bottom).

Therefore less than 80 traces are visible for SI and less than 65 traces for MC events. In this study, the reference time is based on:

- the deflection (i.e., when there is reversed flow from west to east) of solar wind azimuthal velocity (Vy) for an SI arrival at Earth and
- the smooth reversal of IMF Bz from northward to southward when an MC arrives.

3. Results and discussion

3.1 *Geophysical properties of SI and MC-driven dropouts*

Geomagnetic and solar wind properties were investigated and presented in figure 2(a–h). From the selected properties of SI dropouts as shown in figure 2(a–h) (blue lines), some significant characteristics can be seen. In coincidence with gradual dropouts the Kp index (a, blue line) is elevated while it is low prior to the SI triggered dropouts. Although the Kp in OMNI format is seen to be ramping upon –0.8 day, the peak of 4+ is reached in coincidence with the onset of SI arrival at Earth. As Kp, which is the measure of the strength of the solar wind driving the magnetosphere, starts to rise so does the Dst index (b, blue line) starts to drop. At the onset of SI, Dst reverses to modest average of about –30 nT. Dst index is a measure of ring current perturbation and it is expected to be moderate in a typical high speed solar wind stream (Ogunjobi *et al.* 2015). As Dst drops below nominal level, the average of the IMF B_Z (c, blue line) reverses from northward to southward. The northward IMF B_Z interval prior to the onset of SI initiates calm before the storm.

Apparently, this turning would have converts closed electron drift paths outside of GEO to open paths, allowing electrons to be lost through a compressed magnetopause; a process known as magnetopause shadowing. During the southward turning of IMF B_Z, electrons can gain access into the Earth's ionosphere depositing significant amount of their energy resulting in increase in ionospheric ionization. Prior to the arrival of SI, the density (d, blue line) is compressed slow wind and a peak of 17 cm^{-3} is seen on arrival of SI. The increase on the arrival of SI is a clear indication of dynamic pressure difference of the fast wind overtaking the slow wind. The variation in superposed

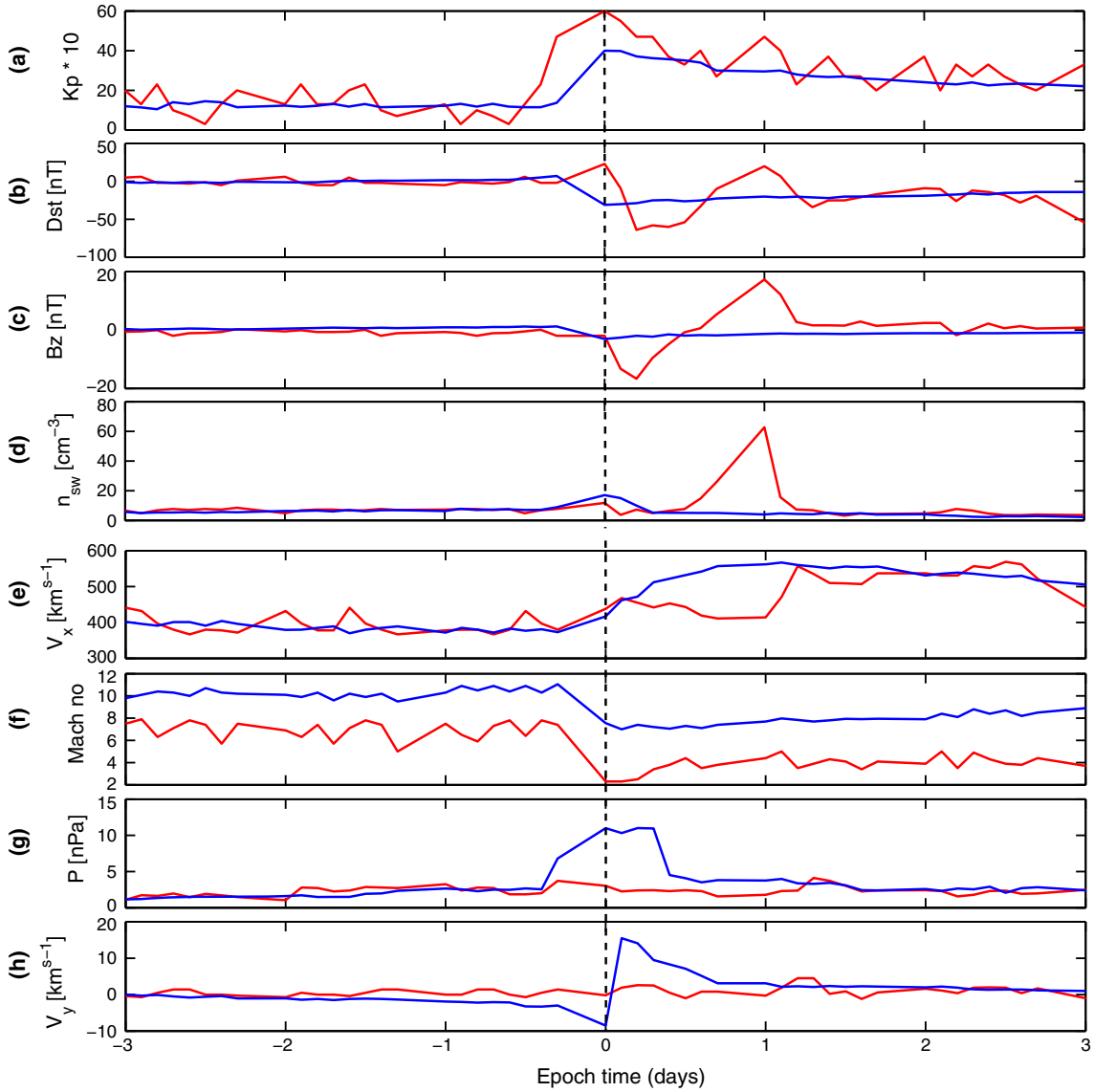

Figure 2. Plots of superposed properties of SI-driven dropouts (blue line) and MC-driven dropouts (red line) used. The zero epoch taken as SI onset are indicated by vertical line. From top is Kp, Dst, IMF Bz, solar wind number density, solar wind radial velocity, Alfvén Mach number, solar wind pressure and the solar wind azimuthal (west–east) flow velocity.

average of solar wind radial velocity (V_X GSE) (e, blue line) compares well with solar wind density. Prior to the onset of SI is low wind speed at the range of ∼400 km/s, which is ramping up closer to arrival of SI. The solar wind is well over 550 km/s after the arrival of SI till over +3 days. The superposed average of Alfvén Mach number, MA (f, blue line) in the solar wind remains high at about 9.3 after the arrival of SI. High Alfvén Mach number is much expected of CIR storm drivers due to high speed solar wind stream. The solar wind pressure (g, blue line) is ramping up few hours prior to the arrival of SI and reaches a peak of about 10 nPa on arrival. In about +0.4 day, the solar wind pressure is seen to have returned to pre-event level. The solar wind azimuthal velocity (h, blue line) reversed past an average of –12 to +19 km/s on arrival of SI. The point of reversal through zero, i.e., the reversal from westward to eastward is taken as SI onset in this study. Any point before the onset is compressed slow wind and after the arrival is compressed fast wind.

Whereas during MC dropouts as presented in figure 2 (red lines), some of the geophysical parameters differ. During the course of the MC dropouts, the ring current is relatively stronger as indicated by a strong depression of Dst at the onset and then gradual recovery. This is indicative of high pressure of the magnetospheric plasma, which is, arguably, caused by an increase in magnetospheric

convection. Dst, however, returns to the pre-event level almost immediately after the MC onset. Such current induction explains the strong presence adiabatic loss process during MC than SI. Contrary to SI driven storms, Alfvén Mach number, MA is lower during the MC driven event. Such disparity in MA and Dst response during SI and MC indicate possible varying operation of the magnetosphere for SI (CIR attendant) and MC (ICME attendant) driven storms (Ogunjobi *et al.* 2015). A good step towards understanding those possible mechanism in operation requires knowledge of energetic particle behaviour from different platforms (GEO, LEO and ground-based instruments) in response to SI and MC events.

3.2 *Characteristics of dropouts at GEO*

Dropouts as earlier stated, is the loss of electrons from the outer radiation belt at the main phase of a storm event and subsequent recovery. Figure 3 presents the superposed multi-satellite average of the logarithm of electron flux from LANL satellites at GEO. Data were obtained from four LANL satellites wherever possible. This is to ensure that all the local times are covered. A running average of the measurement on each was used to construct a multi-satellite logarithmic average of all the fluxes available per time. This is to ensure that all LANL satellites employed have the same yearly averaged logarithm of the flux in the dawn sector. Generally, there is an apparent substorm activity during these events. Nevertheless, the minimal electron flux can be noticed relative to the zero epochs.

In the case of SI, for example, throughout the energy bands, the electron dropout is seen at minimum after the impact of SI (figure 3 blue lines). At the 225–315 keV electron flux band, there is a strong tendency for superposed average of electron flux dropout few hours prior to arrival of SI reaching minima at about 2 hrs after the SI onset. At this band, the effect seems not well pronounced deeper in the magnetosphere and the recovery takes about 0.2 days, but higher than the pre-event level.

The average of 315–500 keV electron flux band also shows a tendency for electron flux dropout reaching deepest minima after the impact of SI. The minimum electron flux time is prolonged for over 4 hrs, after which there is recovery to pre-event level. Dropouts at this energy band are seen to be about 0.8 order deeper than a lower energy band.

At 0.75–1.1 MeV band, the average of electron flux also shows a tendency for dropout, with deepest minima on SI arrival. Dropout continues for about 0.5 day after the arrival. The recovery is slow, taking up to 3 days to return to the pre-event level. The dropout is an average of 1.5 order deeper than the lower energy band.

Again the tendency for electron flux dropout continues within the band of 1.1–1.5 MeV. The minima are seen after the arrival of SI. Dropout

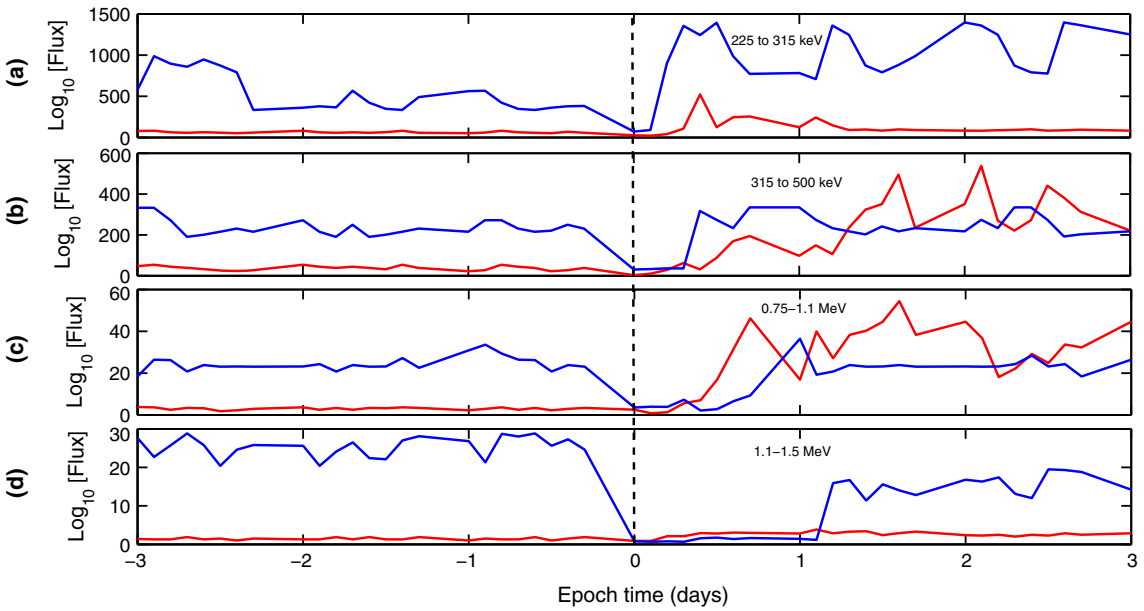

Figure 3. Superposed epoch plots of electron flux during SI-driven dropouts (blue line) and MC-driven dropouts (red line) as measured by combined LANL SOPA satellites: (**a**) 225–315 keV, (**b**) 315–500 keV, (**c**) 0.75–1.1 MeV, and (**d**) 1.1–1.5 MeV.

continues for over 3 hrs. The recovery is very slow and remains less than the pre-event level for more than 3 days after SI arrival.

Overall, the SI dropouts were found to be energy-dependent at all local times, which only recover quickly at lower energy. The prolonged recovery at higher energy band was likely to be that acceleration processes are either weak or dominated by loss processes for the higher electron energies. The tendency for the dropouts begins during compressed slow solar wind while the recovery from dropouts commences during the passage of the compressed fast wind. These processes can be related to an enhanced magnetospheric convection and inward radial diffusion driven by plasma waves in the near-Earth environment (Morley *et al.* 2010). This observation is similar to Borovsky and Denton (2009), which documented typical chronology of a recurring HSSW cycle and the resulting phases of the relativistic-electron dropouts with the suggestion that ion cyclotron waves likely play key role in dropout occurrence. However, the study of Borovsky and Denton (2009) did not test the consistency of such waves during SI and MC dropouts.

Contrary to the SI observation, figure 3 (red lines) shows MC-driven dropout to be independent of energy. Though beginning with local effects, an eventual loss was noticed during MC. The reason for the time scale disparity may be attributed to multiple contributing processes which occurred nearly simultaneously. This is similar to the study of Onsager *et al.* (2002) who investigated the dependence of radiation belt electron dropouts on local time, radial distance, and particle-energy. It was noted that the initial dropouts were controlled by the adiabatic (local) response called Dst effect and that non-adiabatic, which involve interactions with various magnetospheric waves will eventually cause the loss of electrons from the magnetosphere. In this study, the level of dropout is found to correlate with the immediate drop in the Dst and IMF Bz, indicating the presence of adiabatic loss at the MC onset. The real loss is later noticed since the dropout recovery level remains lower when the IMF Bz returned to pre-event level. In other words, the dropouts did not recover with the recovery of IMF Bz and Dst index as presented in figure 3 (red lines). An implication of this is that precipitation or energy deposition at low Earth orbit (LEO) during outer electron dropout can be, partly, employed in the explanation for any mechanism that is more dominant during SI- and MC-triggered dropouts.

3.3 *Deposition of >30 keV electrons*

Using MCETM (Ogunjobi *et al.* 2014a), the deposition of electron flux from POES satellites is analyzed. There is no significant deposition of >30 keV electron counts prior to the arrival of SI as presented in figure 4. However, an abrupt slower decaying peak (about 3000 counts/sec) is seen in the SI arrival within $5.05 < L < 6.05$ (polar region) which persist till 0.5 days before gradual recovery as can seen in figure 4. This is indicative of the existence of relativistic electron microburst. Using GPS measurements, Morley *et al.* (2010) had earlier observed such abrupt decaying peaks. Apparently, relativistic electron precipitation is seen to be taking a form of brief microburst (<1 s) of precipitating electrons and as well as over a wide range of time scales, lasting from minutes to hours. An implication of this is that there were precipitations of electrons during SI over the Polar Regions, which can partly explain the dominant mechanism during dropout interval. Although these regions are outside the portion of the magnetosphere that rotates with the earth (i.e., plasmapause), it is still indicative of the influence of wave-particle interaction: a process whereby the wave fields interact with the particles' momenta and energies resulting in scattering of energetic particles from the outer radiation belt (Tsurutani and Lakhina 1997). One type of such interactive process between a wave and a charged particle is cyclotron wave–particle interaction. Cyclotron waves are of special importance in outer radiation belt physics and have long been suspected of being one of the major contributors to the loss of energetic particles *via* a resonant wave–particle interaction. This process can cause loss of energetic charged particles from the outer radiation belt and eventual precipitation. Also, this phenomenon is due to the existence of a mechanism that provides pitch angle diffusion of the energetic electrons into the lost cone. In such a mechanism, pitch angle scattering will transport electrons from stably trapped orbits into the drift lost cone, and if the pitch angle becomes less than the local bounce lost cone, the electrons are lost to the atmosphere.

For more clarity on the short burst, a superposed averages of >30 keV electrons from POES 15 and 17 (2030–0630 MLT) and POES 16 and 18 (0730–1930 MLT) at 0° (precipitating), 90° (trapped) channels across three spatial cuts ($L = 4.02$, 5.02 and 6.02) were presented as line plots in figure 5. In figure 5 (top panel), electrons at $L = 4.02$ is plotted. A gap over a factor of 5 between trapped

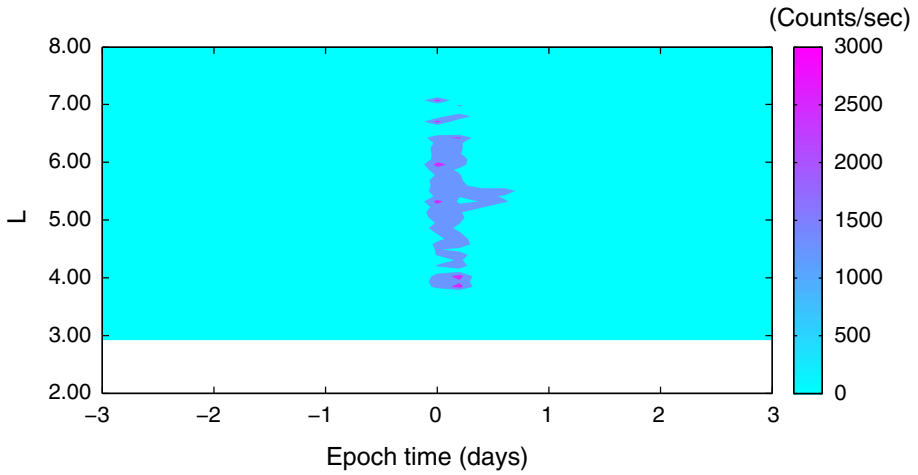

Figure 4. Superposed L-t deposition of >30 keV electron flux from MPED onboard POES satellites during SI-driven dropouts, based on MCETM calculations.

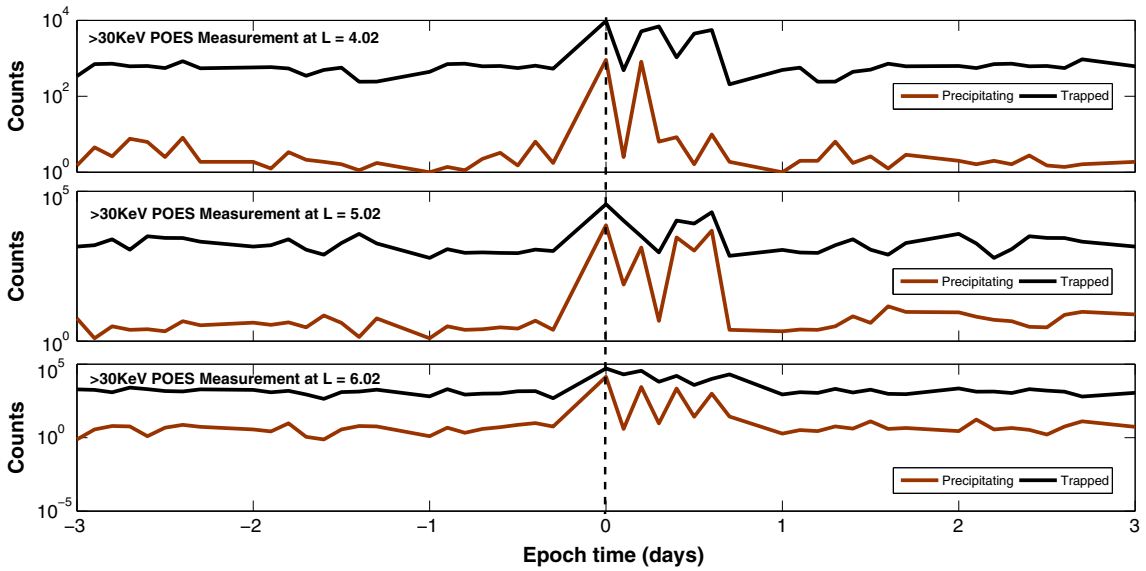

Figure 5. Superposed epoch plot of trapped and precipitating >30 keV electron from NOAA/POES satellite. The black line in each plot indicates measurements from 90° telescope (trapped electrons) while the red line indicates measurements from 0° telescope (precipitating electrons). The dash vertical line indicates arrival of SI (top is the >30 keV at $L = 4.02$, middle is $L = 5.02$ while bottom is counts at L = 6.02).

and precipitating electrons is observed prior-SI and after-SI arrival. At the onset (main phase) of the event, this gap is less, which indicates substantial precipitation on the SI arrival within the dropout intervals. Also of importance is the narrow peak seen on arrival of SI. We continue to observe similar systematic variation in between trapped and precipitating electrons in figure 5 (middle panel) and figure 5 (bottom panel) for the plot of >30 keV electrons at $L = 5.02$ and >30 keV electron at $L = 6.02$, respectively. Generally, the simultaneous slower decaying peak of both trapped and precipitating electrons is seen in the morning sector which began approximately at 0800 MLT to around 1400 MLT. The slower decaying peak lasted for about 6 hrs after the impact of SI. This pattern is an indication of depleted electrons from bounce lost cone *via* a precipitating mechanism known as relativistic 1 MeV) electron microburst (or short-duration bursts of precipitating relativistic electrons) (O'Brien *et al.* 2004; Millan and Thorne 2007; Morley *et al.* 2010; Ogunjobi 2011).

O'Brien *et al.* (2004) showed evidence to pitch-angle of electron microburst precipitation. It was shown that, scattering by a whistler-mode chorus could be the mechanism responsible for relativistic

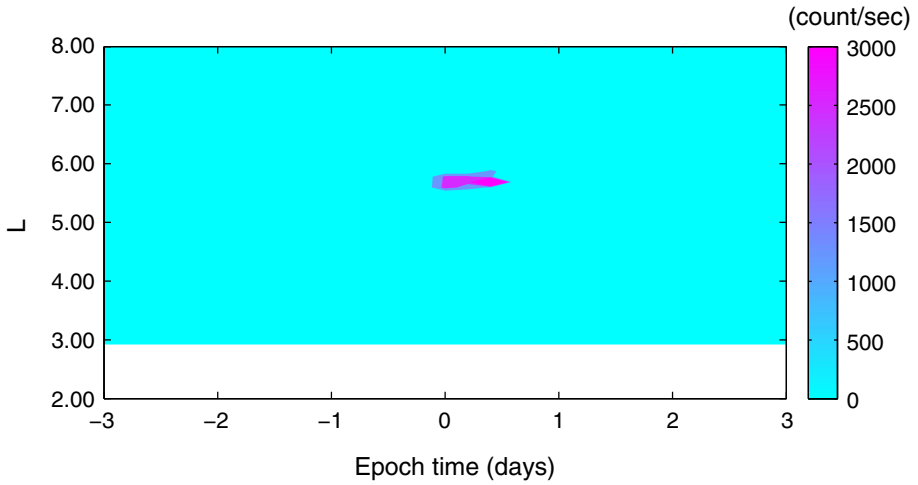

Figure 6. Superposed L–t deposition of >30 keV electron flux from MPED onboard POES satellites during MC-driven dropouts, based on MCETM calculations.

electron microburst, since both are often observed between 0300 and 1500 MLT. In another study, Millan and Thorne (2007), relativistic (>1 MeV) microburst were observed to be correlated with chorus riser due to its likely occurrence between $5 < L < 6$ with losses much stronger during the main phase of geomagnetic activity, and capable of emptying the outer radiation belts in a day or less. Using GPS, Morley *et al.* (2010) in their observational study attributed electron microburst as a responsible mechanism for the observed outer electron dropouts. However, the possibility of EMIC waves which often occurred in the afternoon sector, cannot be completely ruled out. EMIC waves are typically observed at $L > 7$ in the post-noon MLT sector. It is also expected that the minimum energy for pitch-angle scattering of electrons by EMIC should be above 2 MeV (Meredith *et al.* 2003). In this study, we observe dropouts and eventual precipitation of energy below 1 MeV. In this case, however, relativistic electron microburst plays a substantial role during SI triggered dropouts.

On the other hand, energy deposition is seen during MC (figure 6), but in the form of pancake distribution (Wrenn *et al.* 1979; Meredith *et al.* 1999). This distribution extends to region outside and inside plasmapause. According to Wrenn *et al.* (1979), pancakes are the remnants of pitch angle diffusion driven by electron cyclotron harmonic (ECH) waves, depending on the L region. ECH waves can resonate with the outer electrons and have been pointed out as the driving force for pitch angle diffusion of electrons of varying energy (Meredith *et al.* 1999), particularly inside $L = 6$ (in the vicinity of plasmapause) region. For pancake distributions outside $L = 6$, whistler mode waves have been suggested to be the dominant mechanism (Meredith *et al.* 1999). A right hand circularly polarized electromagnetic wave describes the phenomenon known as a whistler mode wave. Therefore, the combinations of ECH and whistler mode waves seem to play significant roles during MC-triggered dropouts. One step way to further confirm this suggestion is to examine riometer absorption across a wide range of L shells as follows.

3.4 *Ionospheric absorption*

In order to ascertain the presence of wave–particle interaction during SI- and MC-triggered geomagnetic storms, we examined the ionospheric absorption. Figure 7(a–h) shows the superposed average of ionospheric absorption throughout the chain of Finish riometers.

Riometer peaks in the region where collision is dominated. In coincidence with POES observation, a superposed average of ionospheric absorption is busty and more localized in the high-latitude at approximately $5 < L < 6$ during SI (figure 7, blue line). Also absorption at approximately $5 < L < 6$ is seen to be delayed for over 3 hrs after the impact of SI. Also, the peaks at these regions coincide with the interval of outer electron dropouts as earlier shown in figure 3. These indicate a strong evidence for relativistic (>1 MeV) electron microburst as the most dominant mechanism during SI triggered dropouts.

Conversely, figure 7 (red line) shows substantial absorption at lower L during MC dropouts. Although we observed prolonged absorption during MC-triggered dropouts. This further

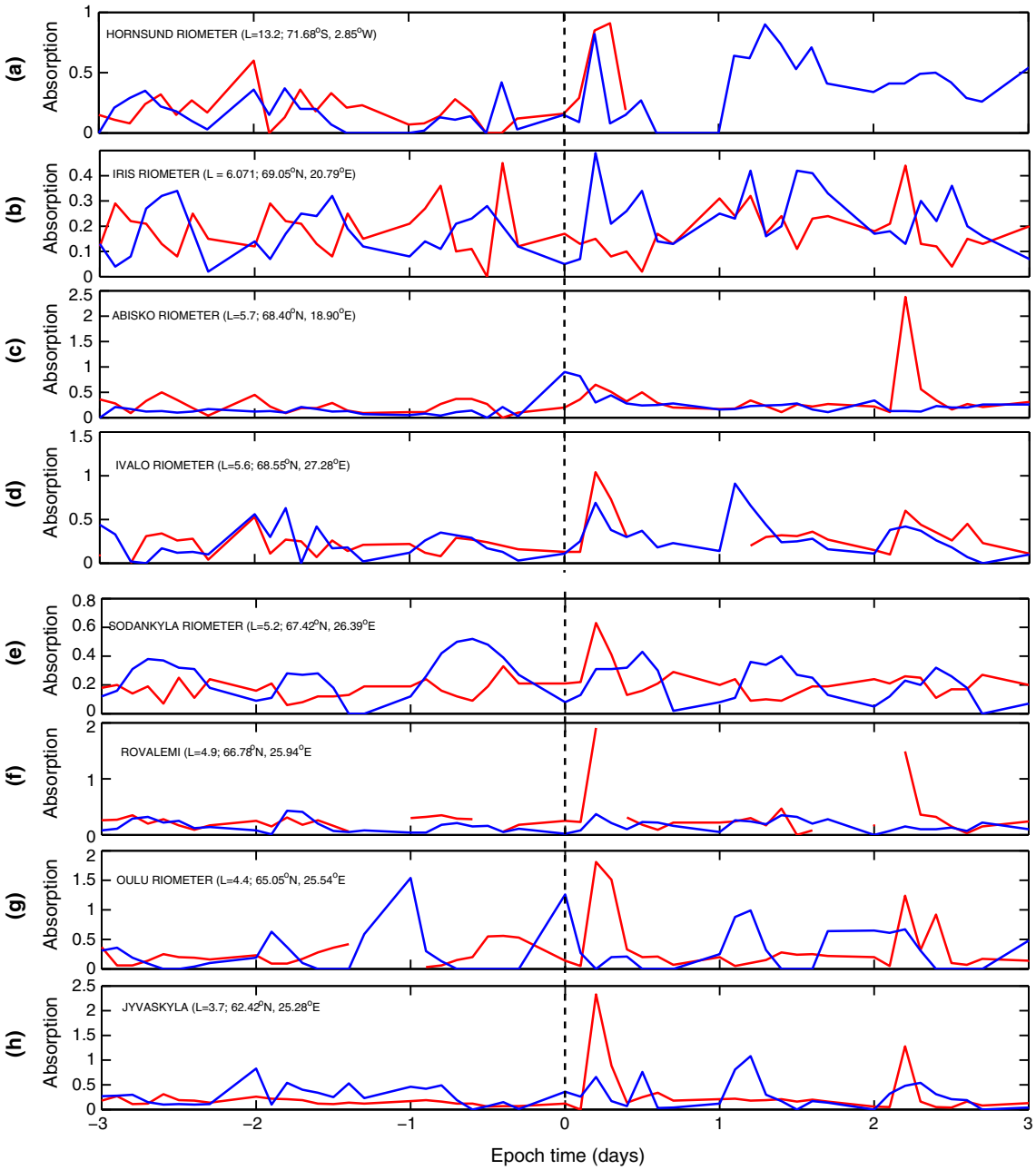

Figure 7. Superposed epoch of individual Finnish riometer absorption during SI-driven dropouts (blue line) and MC-driven dropouts (red line). From (a–h) is Hornsund, Iris, Abisko, Ivalo, Sodankylä, Rovanlemi, Oulu and Jyväskyla. The vertical line indicates onset of events.

confirms the pancake distribution presented in figure 4. It is apparent that the ECH waves can resonate with the outer electrons, hence a driving force for pitch angle diffusion of electrons of varying energy within the region of plasmapause. Also ECH is the mode at which the very low frequency (VLF) signals travel through a plasma medium. This observation confirms the expectation of Tsurutani and Lakhina (1997). It is expected that during magnetic storm recovery phase, any interaction involving whistler-mode chorus waves and radiation belt particles is capable of scattering energetic electrons into the loss cone, resulting in ring current decay and, ultimately, an enhanced upper atmospheric absorption (Ogunjobi *et al.* 2014a).

4. Summary and conclusions

This study analyzed the geophysical characteristics of SI- and MC-triggered storms. The SEA of GEO electron flux dropouts in response to

SI an MC were performed using combined LANL satellites. Also, analysis is presented for average >30 keV electron precipitation during both SI and MC dropouts using POES satellites. Furthermore, an attempt is made to correlate the SI and MC dropouts with the ionospheric absorption using a Finish chain of ground based riometers across the northern hemisphere. The main results emerging from this investigation are as follows:

- The magnetosphere is immersed in compressed slow solar wind a day prior to the arrival of SI. In coincidence with this gradual loss, the Kp index starts to rise, as does the solar wind number density. The resultant increase in solar wind pressure at the onset would have caused the magnetopause to move inward. These gradual losses are consistent with a combination of loss mechanisms provided that the outward radial diffusion also takes place. High Alfvénic magnetic fluctuations contribute to the enhanced magnetospheric condition during SI. On the contrary, MA was low during the course of the MC dropouts; however, the ring current was strong at the onset and then recovers at a slower rate. Such current induction during MC explains the presence of action of the adiabatic lost process.
- On average, the SI dropouts were found to be energy dependent at all local times, which only recover quickly at lower energy. The prolonged recovery at higher energy band was likely to be that acceleration processes are either weak or dominated by lost processes for the higher electron energies. Plausible phenomena which could have led to the observed SI dropouts were noted to be possibly due to an enhanced magnetospheric convection and inward radial diffusion driven by plasma wave near Earth environment. On the other hand, MC driven dropouts were observed to be energy independent. Though beginning with local effects, an eventual loss was noticed during MC. The reason for the time scale disparity may be attributed to multiple contributing processes which occurred nearly simultaneously.
- SEA revealed an unstructured abrupt peak (with slower decaying character) of precipitating >30 keV electron flux from LEO on arrival of the SI which coincided with time of deepest minimum of observed outer electron dropouts from GEO. SEA further reveals $5 < L < 6$ as region of higher precipitation of electron flux during SI dropouts. The slower decaying peak lasted for about 6 hrs after the impact of SI. This pattern is an indication of depleted electrons from bounce lost cone *via* a precipitating mechanism known as relativistic (>1 MeV) electron microburst. In a sharp contrast, energy deposition is seen during MC, but in the form of pancake distribution, which indicates the action of remnants of pitch angle diffusion driven by electron cyclotron harmonic (ECH) waves. This distribution extends to region outside the plasmapause.
- During SI, absorption remains busty between mid- and high-latitude regions. The peaks at these regions coincided with the time of minimal electron flux from LANL and peak of precipitation from POES. This observation is similar to that of Morley *et al.* (2010), which shows busty absorption around $(5 < L < 6)$ at the morning sector. Conversely, we observed absorption at lower L during MC dropouts, although the absorption during MC is also prolonged in comparison with the former event. This observation confirms the expectation of Tsurutani and Lakhina (1997). It is expected that during magnetic storm recovery phase, any interaction involving whistler-mode chorus waves and radiation belt particles is capable of scattering energetic electrons into the loss cone, resulting in ring current decay and ultimately an enhanced upper atmospheric absorption. The results show that SI-triggered storms will, probably, have a greater effect on space-based assets while the MC-triggered storm will, perhaps, have greater impacts on ground-based assets.
- These observations will be taken into account in the ongoing development of our modified half-wave rectifier model for magnetospheric activity.

Acknowledgements

The authors are grateful for the availability of OMNI data provided by the GSFC/SPDF at the OMNIWeb interface, the NOAA/POES at NGDC and Finnish chain of riometers in SGO. The authors also express thanks to JESS anonymous reviewers for their valuable comments and suggestions. This work is based on the research supported in part by the National Research Foundation (NRF) of South Africa.

References

Baker D N, Kanekal S G, Hoxie V C, Henderson M G, Li X, Spence H E, Elkington S R, Friedel R H W, Goldstein J, Hudson M K, Reeves G D, Thorne R M, Kletzing C A and Claudepierre S G 2013 A long-lived relativistic electron storage ring embedded in earth's outer Van Allen belt; *Science* **340** 186–190.

Behera J K, Sinha A, Singh A K, Rawat R, Vichare G, Dhar A, Pathan B M, Nair K U, Selvaraj C and Elango P 2014 First results from imaging riometer installed at Indian Antarctic Station Maitri; *J. Earth Syst. Sci.* **123** 593–602.

Belian R D, Gisler G, Cayton T and Christensen R 1992 High-Z energetic particles at geosynchronous orbit during the great solar proton event series of October 1989; *J. Geophys. Res.* **97** 16,897–16,906.

Borovsky J E and Denton M H 2009 Relativistic-electron dropouts and recovery: A superposed epoch study of the magnetosphere and the solar wind; *J. Geophys. Res.* **114** A02201.

Burlaga L F 1974 Interplanetary stream interfaces; *J. Geophys. Res.* **79** 3717–3725.

Chree C 1908 Magnetic declination at Kew Observatory, 1890–1900; *Phil. Trans. Roy. Soc. London* **A** 205–246.

Fennell J, Roeder J, Spence H, Singer H, Korth A, Grande M and Vampola A 1996 CRESS observations of particle flux dropouts events; *Adv. Space Res.* **18** 217–228.

Horne R B 2007 Acceleration of killer electrons; *Nature* **3** 590–591.

King J and Papitashvili N 2005 Solar wind spatial scales in and comparisons of hourly Wind and ACE plasma and Magnetic field data; *J. Geophys. Res.* **110** A02209.

Lam M M, Horne R B, Meredith N P, Glauert S, Moffat-Griffin T and Green J C 2010 Origin of energetic electron precipitation >30 keV into the atmosphere; *J. Geophys. Res.* **115** A00F08.

Lepping R P, Burlaga L F, Szabo A, Ogilvie K, Mish W, Vassiliadis D, Lazarus A, Steinberg J T, Farrugia C, Janoo L and Mariani F 1997 The wind magnetic cloud and events of October 18–20, 1995: Interplanetary properties and as triggers for geomagnetic activity; *J. Geophys. Res.* **102** 14,049–14,064.

McIlwain C E 1972 Newblock plasma convection in the vicinity of geosynchronous orbit in the Earth's magnetosphere processes; *Earth's Magnetospheric Processes,* pp. 268–279.

Meredith N P, Johnstone A D, Szita S, Horne R B and Anderson R R 1999 "Pancake" electron distributions in the outer radiation belts; *J. Geophys. Res.* **104** 12,431–12,444.

Meredith N P, Thorne R M, Horne R B, Summers D, Fraser B J and Anderson R R 2003 Statistical analysis of relativistic electron energies for cyclotron resonance with EMIC waves observed on CRRES; *J. Geophys. Res.* **108** 1250.

Millan R, Lin R, Smith D, Lorentzen K and McCarthy M 2002 X-ray observations of MeV electron precipitation with a balloon-borne germanium spectrometer; *Geophys. Res. Lett.* **29** 2194.

Millan R and Thorne R 2007 Review of radiation belt relativistic electron losses; *J. Atmos. Sol. Terr. Phys.* **69** 362–377.

Morley S K, Friedel R H W, Spanswick E L, Reeves G D, Steinberg J T, Koller J, Cayton T and Noveroske E 2010 Dropouts of the outer electron radiation belt in response to solar wind stream interfaces: Global positioning system observations; *Proc. Roy. Soc.* **466** 3329–3350.

O'Brien T, Looper M and Blake J 2004 Quantification of relativistic electron microburst loss during the GEM storms; *J. Geophys. Res. Lett.* **31** L04802.

Ogunjobi O 2011 Outer electron radiation belt dropouts: geosynchronous and ionospheric responses; Master's thesis. School of Chemistry and Physics, University of KwaZulu-Natal, Durban, South Africa.

Ogunjobi O, Sivakumar V and Mbatha N 2014a A case study of energy deposition and absorption by magnetic cloud electrons and protons over the high latitude stations: Effects on the mesosphere and lower thermosphere; *Terr. Atmos. Oceanic Sci.* **25** 219–232.

Ogunjobi O, Sivakumar V and Sivla W T 2014b A superposed epoch study of the effects of solar wind stream interface events on the upper mesospheric and lower thermospheric temperature; *Adv. Space Res.* **54** 1732–1742.

Ogunjobi O, Sivakumar V, Stephenson J and Sivla W T 2015 Evidence of polar mesosphere summer echoes observed by SuperDARN SANAE HF radar in Antarctica; *Terr. Atmos. Oceanic Sci.* **26** 431–440.

Onsager T G, Rostoker G, Kim H J, Reeves G D, Obara T, Singer H J and Smithtro C 2002 Radiation belt electron flux dropouts: local time, radial and particle-energy dependence; *J. Geophys. Res.* **107** 1382.

Rodger C J, Clilverd M A, Seppälä A, Thomson N R, Gamble R J, Parrot, M, Sauvaud J A and Th U 2010 Radiation belt electron precipitation due to geomagnetic storms: significance to middle atmosphere ozone chemistry; *J. Geophys. Res.* **115** A11320.

Roeder J 1970 Dynamics of geomagnetically trapped radiation; *Springer-Verlag, New York*, 160p.

Thomsen M F, Bame S, McComas D, Moldwin M and Moore K 1994 The magnetospheric lobe at geosynchronous orbit; *J. Geophys. Res. Lett.* **99** 17283.

Thorne R M, O'Brien T, Hprits Y Y, Summers D and Horne R B 2005 Timescale for MeV electron microburst loss during geomagnetic storms; *J. Geophys. Res.* **110** A09202.

Tsurutani B T and Lakhina G S 1997 Some basic concepts of wave-particle interactions in collisionless plasmas; *Rev. Geophys.* **35** 491–502.

Van-Allen J A 1959 The geomagnetically trapped corpuscular radiation; *J. Geophys. Res.* **64** 1683–1689.

Varotsou A, Friedel R, Reeves G, Lavraud B, Skoug R, Cayton T and Bourdarie S 2008 Characterization of relativistic electron flux rise times during the recovery phase of geomagnetic storms as measured by the NS41 GPS satellite; *J. Atmos. Sol. Terr. Phys.* **70** 1745–1759.

Wrenn G, Johnson J F E and Sojka J 1979 Stable 'pancake' distributions of low energy electrons in the plasma trough; *Nature* **279** 512–514.

Corresponding editor: K Krishnamoorthy